7-2005

# A Multi-Instrument Study of the Helix Nebula Knots with the *Hubble Space Telescope*

C. R. O'Dell
*Vanderbilt University*

W. J. Henney
*UNAM Campus Morelia, Mexico*

Gary J. Ferland
*University of Kentucky*, gary@uky.edu

# A Multi-Instrument Study of the Helix Nebula Knots with the *Hubble Space Telescope*

Digital Object Identifier (DOI)
https://dx.doi.org/10.1086/430803

Notes/Citation Information
Published in *The Astronomical Journal,* v. 130, no. 1, p. 172-187.

The Astronomical Journal, 130:172–187, 2005 July


# A MULTI-INSTRUMENT STUDY OF THE HELIX NEBULA KNOTS WITH THE *HUBBLE SPACE TELESCOPE*[1,2]

C. R. O'Dell
Department of Physics and Astronomy, Vanderbilt University, Box 1807-B, Nashville, TN 37204; cr.odell@vanderbilt.edu

W. J. Henney[3]
Centro de Radioastronomía y Astrofísica, UNAM Campus Morelia, Apartado Postal 3-72, 58090 Morelia, Michoacán, Mexico

AND

G. J. Ferland
Department of Physics, University of Kentucky, Lexington, KY 40506
*Received 2005 February 21; accepted 2005 April 1*

## ABSTRACT

We have conducted a combined observational and theoretical investigation of the ubiquitous knots in the Helix Nebula (NGC 7293). We have constructed a combined hydrodynamic + radiation model for the ionized portion of these knots and have accurately calculated a static model for their molecular regions. Imaging observations in optical emission lines were made with the *Hubble Space Telescope*'s STIS, operating in a ''slitless'' mode, complemented by WFPC2 images in several of the same lines. The NICMOS camera was used to image the knots in $H_2$. These observations, when combined with other studies of $H_2$ and CO, provide a complete characterization of the knots. They possess dense molecular cores of densities about $10^6$ cm$^{-3}$ surrounded on the central star side by a zone of hot $H_2$. The temperature of the $H_2$-emitting layer defies explanation either through detailed calculations for radiative equilibrium or through simplistic calculations for shock excitation. Farther away from the core is the ionized zone, whose peculiar distribution of emission lines is explained by the expansion effects of material flowing through this region. The shadowed region behind the core is the source of most of the CO emission from the knot and is of the low temperature expected for a radiatively heated molecular region.

*Key word:* planetary nebulae: individual (NGC 7293)

*Online material:* color figure

## 1. INTRODUCTION

A pressing issue within the study of planetary nebulae (PNe) is the nature of the highly compact, neutral core knots that have been found in all the nearby PNe studied by the *Hubble Space Telescope* (*HST*) and are arguably ubiquitous (O'Dell et al. 2002, hereafter O02). Their origin is not established, although two extreme models exist. In the first, they originate as knots in the extended atmosphere of the precursor central star (Dyson et al. 1989; Hartquist & Dyson 1997); the second possibility is that they are the results of instabilities occurring at the boundary between the ionized and neutral zones within the nebulae (Capriotti 1973). Perhaps the most significant issue about them is not their origin, but rather their fate. This is because their survival beyond the PN stage would mean that a large fraction of the material being put into the interstellar medium (ISM) by the PN phenomenon would be trapped in optically thick knots, which would then become a new component of the ISM. However, to delve into their origin or prognosticate their future, we must understand the objects as they are now. Fortunately, these knots have become the subjects of recent observational studies that probe from the outside to the inside of the knots, and we can begin to hope to have a complete picture of their nature. This paper presents new observational results for the nearest bright PN, NGC 7293 (the Helix Nebula), that probe both the outer ionized layers and a portion of the neutral inner core of its knots. These observations are then compared with new, sophisticated models that accurately model the regions of origin of the emission, and we present a general model for the objects.

The Helix Nebula is a member of the polypolar class of PN in which there is a smaller filled inner disk within a fainter outer disk that is almost perpendicular to it (O'Dell et al. 2004, hereafter OMM04). The outer disk is open in the middle where it encloses the inner disk, and its opening is surrounded by a brighter feature called the outer ring. Both are optically thick to ionizing Lyman continuum (LyC) radiation. The innermost portion of the inner disk contains a core of $He^{++}$ emission, whose lack of ions with high emissivity gives the nebula a superficial appearance of having a central cavity (O'Dell 1998, hereafter O98). The several thousand knots that are present in the Helix Nebula begin to be seen about the region of transition from $He^{++}$ to $He^{+}$, and they are found with increasing concentration as one moves toward the ionization boundary, both in the inner disk and in the outer ring (OMM04).

The knots were originally discovered by W. Baade and first reported on by Zanstra (1955) and Vorontzov-Velyaminov (1968). The next big step in the illumination of the knots was the paper by Meaburn et al. (1992, hereafter M92), which established that the knots had highly ionized cusps of about 2″ in size facing the hot central star and little emission in the [O III] emission line, and that the dust in their central cores blocked out some of the

[1] Based in part on observations with the NASA/ESA *Hubble Space Telescope*, obtained at the Space Telescope Science Institute, which is operated by the Association of Universities for Research in Astronomy (AURA), Inc., under NASA contract NAS 5-26555.

[2] Based in part on observations obtained at the Cerro Tololo Inter-American Observatory, which is operated by AURA, Inc., under a cooperative agreement with the National Science Foundation.

[3] Work carried out in part while on sabbatical at the Department of Physics and Astronomy, University of Leeds, Leeds LS2 9JT, UK.

background nebular emission, the amount of this extinction providing information about their location within the nebula. This picture was extended by much higher spatial resolution images made with the *HST*, which has now covered several portions of the nebula in the northern quadrant (O'Dell & Handron 1996, hereafter OH96; O'Dell & Burkert 1997, hereafter OB97) and, with lower signal-to-noise ratio, a section in the main ring of emission to the northwest of the central star (O02). There are about 3500 knots in the entire nebula (OH96), and the characteristic mass of each is about $3\times10^{-5}\,M_\odot$ (OB97) or $\gtrsim1\times10^{-5}\,M_\odot$ (Huggins et al. 2002, hereafter H02), the former value meaning that the knots contain a total mass of about 0.1 $M_\odot$, which is about the same as all the ionized gas. This indicates that the knots represent an important ingredient in the mass-loss process of this PN. The *HST* Wide Field Planetary Camera 2 (WFPC2) allowed distinguishing between the low-ionization [N II] emission and that of H$\alpha$ and [O III]. This information, together with slitless spectra (O'Dell et al. 2000, hereafter OHB00), established that the ionization structure of the bright knots was dissimilar to other photoionized structures in that the [N II] structure is more diffuse than that in H$\alpha$, which could be explained by the rather ad hoc introduction of a peculiar electron temperature distribution, which is now explained by the dynamical model introduced in this paper. The inner knots show well-defined "tails," which has led to the knots sometimes being called "cometary knots." The radial alignment of these features has suggested to some authors that there may be a radial outflow of material along them (Dyson et al. 1993), although the shadowing of ionizing LyC radiation must play an important role (Cantó et al. 1998; O'Dell 2000).

The regions within the bright ionized cusps have been probed by observations of their molecular cores, which now have sufficient resolution to make a clear delineation of the emission as arising from the core of the knots, rather than from an extended photon-dominated region (PDR) lying outside the ionization front of the nebula. The entire Helix Nebula has been imaged (Speck et al. 2002, hereafter S02) in the $H_2$ 2.12 $\mu$m line at a resolution of about 2″. This study is supplemented by a 1.″2 resolution image of one of the knots by H02. Radio observations in other molecules have been of progressively better spatial resolution, with the entire nebula having now been mapped at 31″ in CO by Young et al. (1999, hereafter Y99), where the presence of multiple velocity components within the beam indicates that there were emitting regions smaller than the beam size. H02 made CO observations with an elliptical beam of $7.''9\times3.''8$ of the same knots as in their high-resolution $H_2$ study. A splendid spectroscopic study at 6″ spatial resolution of multiple $H_2$ emission lines established (Cox et al. 1998) that the $H_2$ levels are in statistical equilibrium and that the temperature of the $H_2$ portions of the cores is a surprising 900 K. The best resolution study of neutral hydrogen is that of Rodríguez et al. (2002), although their $54.''3\times39.''3$ beam was insufficient to distinguish between emission coming from within the knots and from the PDR associated with the nebula's ionization front.

Fortunately, we know a lot of the basic characteristics of the system. The trigonometric parallax of Harris et al. (1997) indicates that the distance is 213 pc, which means that $1'' = 3.19\times10^{15}$ cm and the 500″ semimajor axis of the inner disk (OMM04) corresponds to 0.52 pc. The dynamic age of the inner disk is 6600 yr (OMM04). The central star has been measured accurately in the far-ultraviolet (the ultraviolet flux with frequencies below the Lyman limit) by Bohlin et al. (1982), who found an effective temperature of 123,000 K. At 213 pc distance the star must have a bolometric luminosity of 120 $L_\odot$. The central region has also been measured in the X-ray region from 0.1 to 2 keV by Leahy et al. (1994), who not only measured radiation from the central star but also found an additional slightly extended source with a temperature of $8.7\times10^6$ K and a total flux of $9\times10^{-14}$ ergs cm$^{-2}$ s$^{-1}$, which converts to a total luminosity of the nonstellar source of $1.3\times10^{-4}\,L_\odot$. There is no spectroscopic evidence (Cerruti-Sola & Perinotto 1985) for continued outflow from the central star, which is consistent with the late evolutionary stage of the star and the observation that there is not a central cavity in the nebular disk.

A note on nomenclature is in order. Various names have been used for the same features in the multitude of papers addressing the Helix Nebula, this nomenclature often reflecting the background of the author and the state of knowledge. The compact features have been called filaments, globules, and cometary knots. In this paper they are called simply "knots." There have also been a variety of names applied to the large-scale bright structures within the bright ring seen in low-ionization-line images that led to the original designation as the Helix Nebula. In this paper we refer to these as "loops." Whenever a fine-scale feature, such as a knot, is to be designated specifically, we use the coordinate-based system introduced in OB97, which avoids the confusion of serial or discovery time–based naming systems.

We describe the new *HST* observations in § 2. Analysis of the images is given in § 3. In § 4 we discuss these observations, showing that the optical line properties require inclusion of the effects of advection and that no model of the knots is able to explain the $H_2$ observations of this or other well-studied PNe.

## 2. OBSERVATIONS

The prime target of the observing program (GO-9489 in the Space Telescope Science Institute [STScI] designation) was the isolated knot 378-801 (OB97 system; C1 in Huggins et al. [1992]; feature 1 in Fig. 3*a* of Meaburn et al. [1998], hereafter M98), which lies nearly north of the central star and on the inside edge of the ring of low-ionization emission lines. It was natural to select this target because of the smooth background of the nebular emission, which makes it easy to correct for that contaminating emission, and because it has been the subject of multiple previous studies, including *HST* imaging (OH96), *HST* low-resolution spectroscopy (OHB00), ground-based high-resolution spectroscopy (M98; O02), and the highest resolution imaging in CO and $H_2$ (H02). The knot lies in a direction of position angle (P.A.) 356° from the central star.

### 2.1. *Spectroscopic Observations*

This knot was observed with the Space Telescope Imaging Spectrograph (STIS; Woodgate et al. 1998) through its $2''\times52''$ entrance slit. Since the bright cusp of this knot is smaller than the width of the entrance slit and the radiation is dominated by emission lines, the STIS was able to form monochromatic images in the various lines, essentially functioning as a slitless spectrograph. This pointing was the same as that employed in program GO-7286. The location of the entrance slit as projected on the nebula is shown in Figures 1 and 2. Because of the paucity of candidate guide stars, the slit was oriented with P.A. = 6°, as were the observations in program GO-7286.

Observations were made with multiple tilts of gratings G430M and G750M. A central wavelength setting of 4961 Å (2340 s exposure) gave useful observations of the H$\beta$ $\lambda$4861 and [O III] $\lambda\lambda$4959, 5007 lines. A central wavelength setting of 6252 Å (4620 s exposure) gave useful observations of the

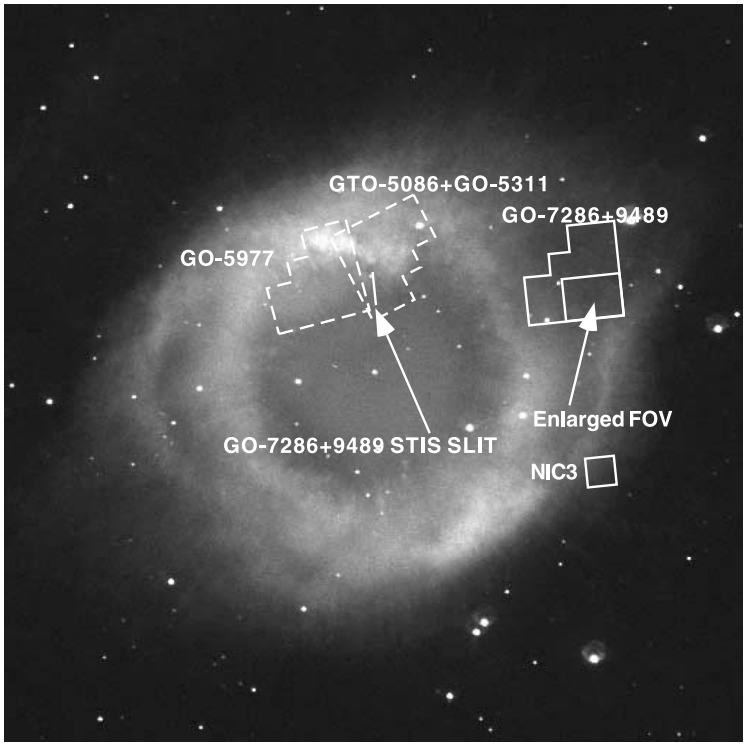


FIG. 1.—Image of the Helix Nebula in H$\beta$ (O98), showing the location of the apertures of the several data sets used in this study and the *HST* program number that led to their creation. This figure is similar to Fig. 7 in O02, except that the correct position angle of the STIS slit (P.A. $= 6^{\circ}$) is shown and the WFPC2 and NIC3 coordinated parallel fields are shifted accordingly. The image is $1180'' \times 1180''$, and north is up.

[O I] $\lambda\lambda$6300, 6363 doublet. A central wavelength setting of 6581 Å (4620 s) gave useful observations of the same [O I] lines, the H$\alpha$ line at 6563 Å, and the adjacent [N II] $\lambda\lambda$6548, 6583 doublet. These images were pipeline-processed by the STScI and flux-calibrated using their system that is tied to observations of standard stars through the same instrument configuration. The resulting images have pixel sizes of 0.″05.

### 2.2. *Imaging Observations*

The wide field of good focus and large data storage capability of the *HST* allow the making of parallel observations. WFPC2 (Holtzman et al. 1995) and NICMOS (Thompson et al. 1998) observations were made during all the primary target STIS observations. Since the primary target determines the pointing of the spacecraft, one gets what is available in terms of the parallel observations. However, the STIS slit could be placed in two orientations of 180° difference. We chose an orientation of the slit so that both the WFPC2 and NICMOS fields would fall onto the main body of the nebula. The WFPC2 parallel field falls in a region outside of the main bright ring of emission of the Helix and in the zone that may be the projection of the more distant rotational axis of the nebula, which is a thick disk accompanied by perpendicular low-density plumes (O98; M98).

#### 2.2.1. *WFPC2 Observations*

We made WFPC2 images of the field shown in Figure 1 in four filters. There were six exposures in F656N for a total exposure time of 5600 s, six exposures in F658N (6600 s total), four exposures in F502N (4000 s total), and three exposures in F547M (300 s total). The multiple exposures were made to allow us to eliminate random events caused by cosmic rays. The F502N filter primarily isolates [O III] $\lambda$5007 emission, while F656N is dominated by H$\alpha$ $\lambda$6563 emission, and F658N is dominated by [N II] $\lambda$6583 emission. However, each filter is affected by the underlying continuum, and the F656N and F658N filters are both affected by H$\alpha$ and [N II] emission, the latter becoming important in the innermost knots, which have much stronger [N II] emission than H$\alpha$ emission. These observations were pipeline-processed at the STScI, then combined with a similar set of observations made during program GO-7286, where the pointing was almost identical and the total exposure times were 4200 s (F502N), 300 s (F547M), 4600 s (F656N), and 2200 s (F658N). These images were then rendered into monochromatic, calibrated emission-line images using the technique of O'Dell & Doi (1999), which corrects each filter for (any) contaminating nonprimary line and the continuum and gives an image whose intensity units are photons cm$^{-2}$ s$^{-1}$ sr$^{-1}$.

The H$\alpha$ and [N II] images are shown in Figure 3. There are many indications of knots of emission, although only a few well-defined bright cusps are seen. The features are much sharper in H$\alpha$ than in [N II], an unusual trend that is consistent with the result found in an earlier study using both slitless spectroscopy and imaging (OHB00). The bottom panel of Figure 3 gives a comparison of the *HST* WFPC2 images with a ground-based H$\alpha$ + [N II] image made with the MOSAIC camera of the 4 m Blanco telescope at the Cerro Tololo Inter-American Observatory (CTIO). This image was made during a period of astronomical seeing with a measured FWHM $= 0.''9$ and a pixel size of 0.″27. We see that the bright regions of about 15″ diameter are broken up into multiple and often overlapping bright cusps with chord sizes of about 2″. The image shows only diffuse faint emission in [O III], which is not surprising since it lies outside of the primary zone of [O III] by the nebula and the knots are known to emit little energy in this ion (M92; OH96; OHB00).

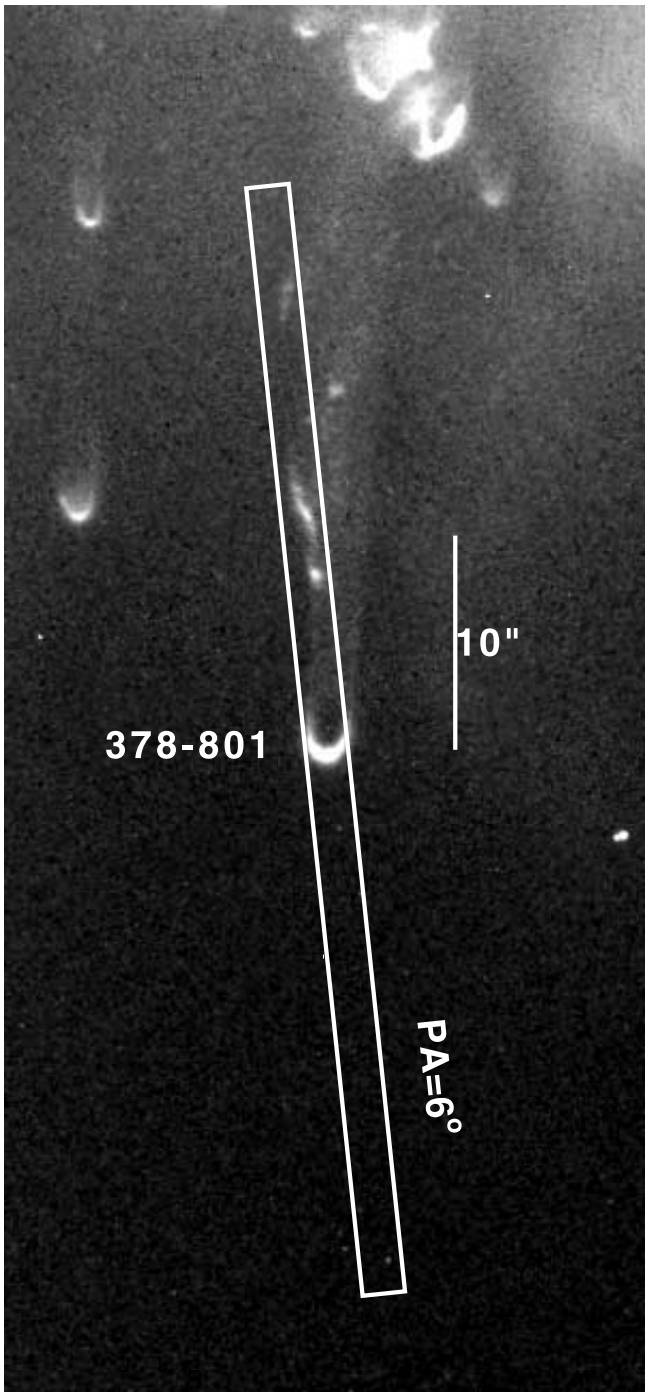


FIG. 2.—A $30'' \times 65''$ section of the sum of the GTO-5086 and GO-5311 flux-calibrated observations of H$\alpha$ and [N II], with the knot 378-801 near the center. The rectangle indicates the boundary of the $2'' \times 52''$ slit used for the STIS observations discussed in this paper. North is up. The features about $10''$ north of the bright cusp of 378-801 may be structure in the tail of this knot or may be a second knot that falls within the radiation shadow of 378-801.

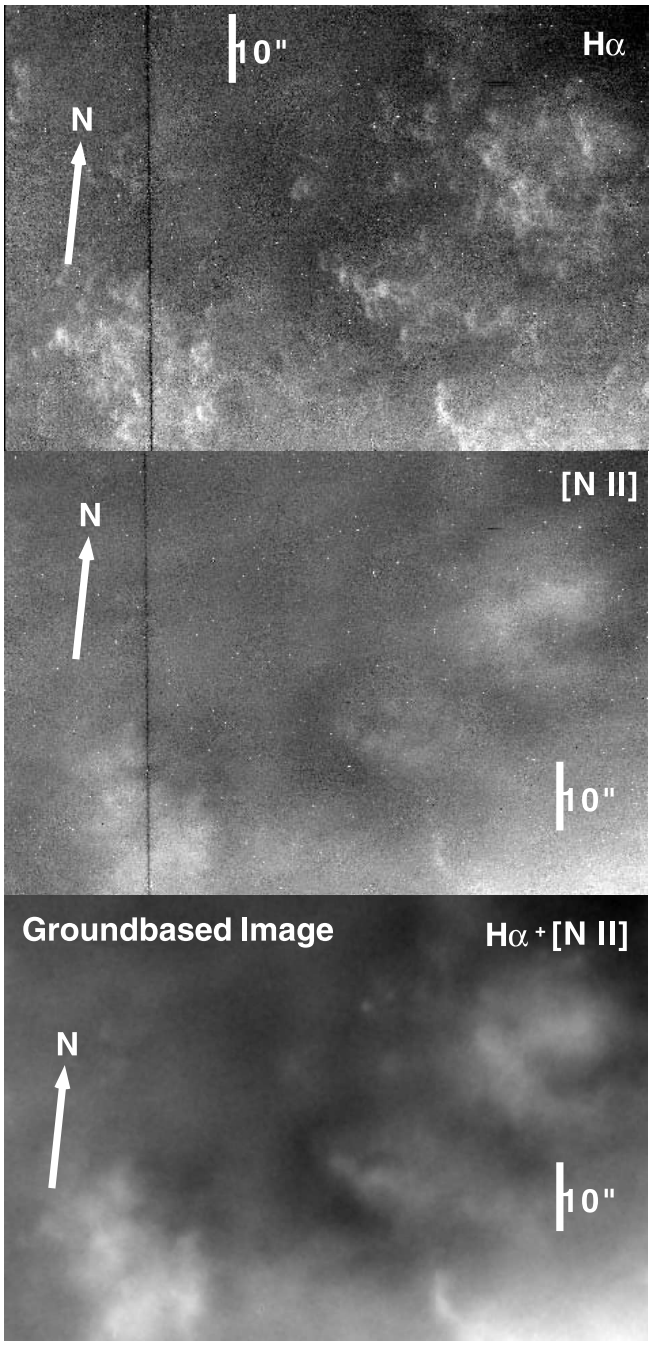


FIG. 3.—*Top, middle*: Portions of the combined images in H$\alpha$ and [N II] created in programs GO-7286 and GO-9489. The field of view of each is $95'' \times 66''$, and the vertical axis is pointed toward P.A. $= 6^\circ$. Contrary to most images of photoionized nebulae, the knots are much sharper in H$\alpha$. The vertical dark line is caused by the seam between WFPC2's CCD2 and CCD3. *Bottom*: Same field in an unpublished H$\alpha$ + [N II] image made by C. R. O. with the MOSAIC camera on the CTIO 4 m telescope under seeing conditions of FWHM $= 0''.9$.

#### 2.2.2. *NICMOS Observations*

We also made parallel observations with all three cameras of the NICMOS instrument. Because of the filter combinations available and the lack of simultaneous focus, in part due to an error in the observing program, only the NIC3 detector results were useful for this study, and even its images are out of focus. That camera has an array of $256 \times 256$ pixels, each subtending $0''.2 \times 0''.2$. We made four exposures (total exposure time of 10,752 s in each) in both the F212N filter and the F215N filter. The F212N filter primarily isolates the $H_2$ 2.12 $\mu$m line and the F215N filter the adjacent continuum. The field imaged is shown in Figure 1 and is almost identical with the field observed in program GO-7286. These new images were not averaged with the older data, because there is always a certain amount of degradation of resolution in combining two not-identical-pointing images, the new images have better spatial resolution, and the earlier observations were of only 3326 s (F212N) and 3582 s (F215N).

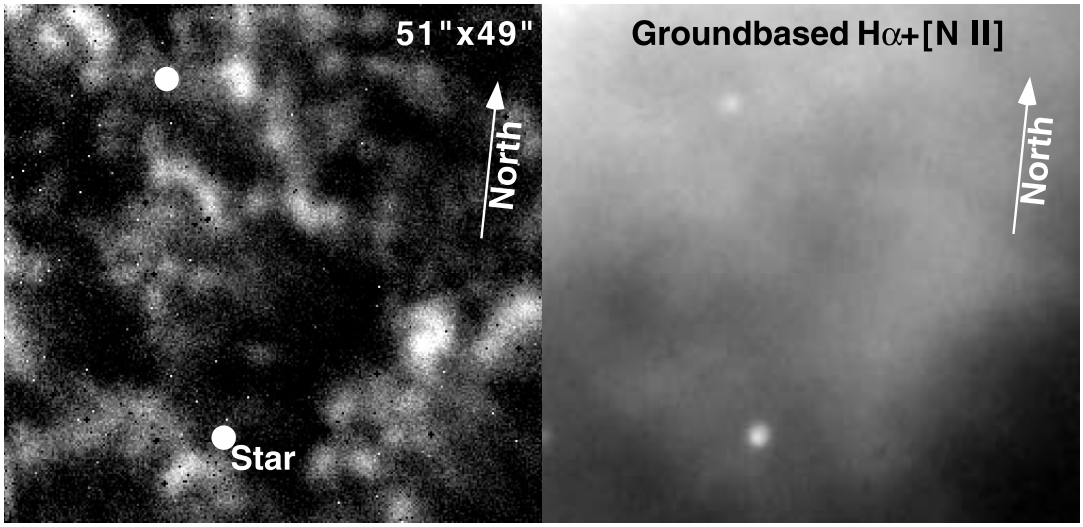


FIG. 4.—*Left*: Out-of-focus $51'' \times 49''$ NIC3 parallel image in continuum-subtracted values of $S_{2.12\ \mu m}$. The image has been rotated so that the vertical axis is at P.A. $= 6^\circ$ in order to nearly match the orientation shown in Fig. 1. The average value of $S_{2.12\ \mu m}$ is $1.0 \times 10^{-5}$ ergs s$^{-1}$ cm$^{-2}$ sr$^{-1}$, and the peak value is $4 \times 10^{-5}$ ergs s$^{-1}$ cm$^{-2}$ sr$^{-1}$. Correction of the peak values of $S_{2.12\ \mu m}$ for the instrumental FWHM being greater than the cusp-shaped area of the emitting regions is discussed in the text. The characteristic FWHM of the stars is about $1''.8$. *Right*: Matching field from the same H$\alpha$ + [N II] image as in Fig. 3.

The NIC3 images are significantly out of focus, but some information can be obtained from them. The stars in our field of view have central dips of about 30% and an FWHM value of 9 pixels. This means that we cannot hope to resolve nebular $H_2$ structures of less than $1''.8$.

The images were subjected to the STScI's pipeline data processing, which gave corrected count rates (CRs) per pixel in each detector. The instrument data handbook (§ 5.3.4) gives, for the calibrated flux (in ergs s$^{-1}$ cm$^{-2}$) from an emission line, flux $= 1.054 \times$FWHM$\times$PHOTFLAM$\times$CR, where FWHM is that of the filter and PHOTFLAM is a sensitivity constant determined from observations of a calibrated continuum source. In using this equation the assumption has been made that the emission line is at the center of the filter (a good assumption for this low-velocity source) and that the continuum contribution has been subtracted (discussed in this section). Inserting the tabulated values of FWHM $= 202$ Å and PHOTFLAM $= 2.982 \times 10^{-18}$ gives flux $= 6.35 \times 10^{-16}$. We corrected for the continuum by examination of a section of the image that contained no evidence of knots, normalizing the F215N filter signal to be the same as the F212N image in that section, then subtracting the normalized F215N image from the F212N image. After scaling into surface brightness ($S_{2.12\ \mu m}$ in ergs s$^{-1}$ cm$^{-2}$ sr$^{-1}$) and trimming a bad edge, one has the image shown in Figure 4, where the average value of $S_{2.12\ \mu m}$ is $1.0 \times 10^{-5}$ ergs s$^{-1}$ cm$^{-2}$ sr$^{-1}$ and the peak value is $4 \times 10^{-5}$ ergs s$^{-1}$ cm$^{-2}$ sr$^{-1}$. The intrinsic values of $S_{2.12\ \mu m}$ will be higher by an amount determined by the defocus. However, we should be able to determine accurate total fluxes for the individual knots. These points are addressed in § 4.3, in which we also compare our values with ground-based observations.

## 3. ANALYSIS

### 3.1. *Analysis of the WFPC2 Images*

Studies of the variation in the peak surface brightness of the cusps with angular distance from the central star have been made previously (OH96; López-Martín et al. 2001) with the expectation that this would be a useful diagnostic of the knots. This is because each cusp represents a local ionization front and, to first order, their surface brightness in a recombination line such as H$\alpha$ should scale linearly with the incident flux of LyC photons, as long as the cusps are in static ionization equilibrium with recombinations balancing photoionizations. OH96 demonstrated that the cusps were significantly fainter than expected from this simple argument, and López-Martín et al. (2001) found from the careful study of a few knots that this deficit of emission could be explained by advection of neutral hydrogen from the core into the cusp, which represents an additional sink of ionizing photons and leads to a reduced rate of recombinations compared to the static case.

In light of the fact that we now have calibrated H$\alpha$ and [N II] data that cover a much wider range of angular distances from the central star than in other studies, we have reexecuted an analysis of the brightness of the cusps. We have measured the peak cusp surface brightness for 530 knots identified in the WFPC2 fields of programs GTO-5086, GO-5311, and GO-5977 (OH96; OB97) and an additional 70 in the WFPC2 field obtained in this study (§ 2.2.1). The brightness of each cusp was measured in a $2 \times 5$ pixel box centered on the brightest portion and oriented with the long axis perpendicular to a line toward the central star. The nebular surface brightness used for correction of the cusp signal was determined from a nearby $5 \times 10$ pixel box. A similar analysis of the [N II] image was done for each object, but the cusp sample box was shifted 0.8 pixels toward the central star. The knot cores were also sampled in [O III] using $5 \times 5$ pixel boxes that were shifted 7 pixels away from the central star with respect to the H$\alpha$ cusp.

The results for H$\alpha$ of this analysis are shown in Figure 5. In this figure we show the surface brightness for H$\alpha$ and the standard deviation of the nearby nebular emission for a box of the same size as that used for extracting the cusp brightness. The results indicate that we have traced the cusps out to where they are lost in the fluctuations of the nebular background. The solid line is the expected relation if all the knots are viewed face-on and located at the distance indicated by their angular separation (these are mutually exclusive conditions). This is the same method of calculation as that of OH96, except that the more recent value of the total flux of the nebula of $F(\mathrm{H}\beta) = 3.37 \times 10^{-10}$ ergs cm$^{-2}$ s$^{-1}$ (O98) is used. This method of

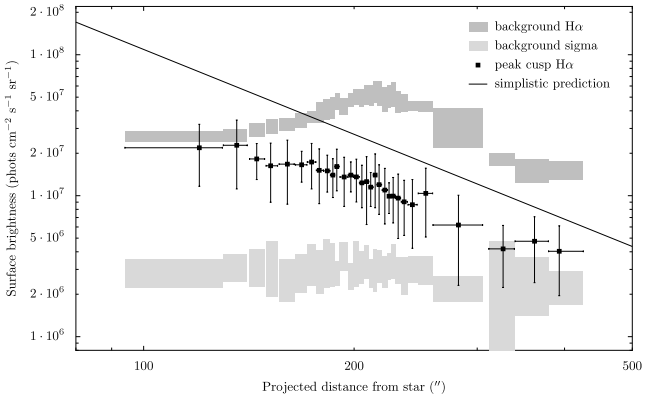


FIG. 5.—Peak H$\alpha$ surface brightness of the knot cusps (*squares*), the nebular brightness (*dark-gray boxes*), and the standard deviation of the nebular brightness (*light-gray boxes*) as a function of the distance from the central star. The boundaries of the boxes indicate the 1 $\sigma$ boundaries about the mean values. The solid line is the predicted relation under the assumptions of the knots being viewed face-on, the distance from the central star being that indicated by the angular separation, and diminution of LyC radiation by advected neutral hydrogen being unimportant. In the case of failure of each of these assumptions, the expected surface brightness would be lower than this prediction.

calculation also ignores the effects of advection. In practice, few of the knots will be viewed in the plane of the sky. Most will be at foreground or background positions that will place them farther from the central star than indicated by their angular separations, and some advection will be present. Each of these factors will cause the expected surface brightness to be less than the line labeled "simplistic predictions." Limb brightening would tend to work in the opposite direction by raising the cusp brightness, but this is evidently less important than the first two effects.

The characteristics of the nebula and the knots in [N II] are summarized in Figure 6, in which we see that the cusp brightnesses monotonically decrease with increasing distance from the central star, while the nebular brightness peaks at about 210″. The nebula's peak is due to reaching the ionization front that confines the inner disk and outer ring, these being seen at about the same distance from the central star in the northern sector (OMM04), which numerically dominates this sample. It is difficult to determine a trend of [O III] emission from in front

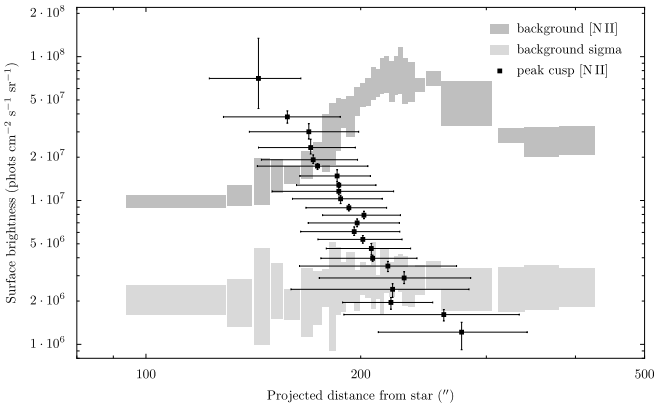


FIG. 6.—Similar to Fig. 5, but presenting the results of the analysis of [N II]. In addition to the [N II] for the cusps (*squares*), we also give the values for nearby portions of the nebula (*dark- and light-gray boxes*). The cusp [N II] emission becomes weaker at greater distances, and the nebular emission shows a relative increase. Negative values indicate that the [N II] appears fainter than the nebular surroundings.

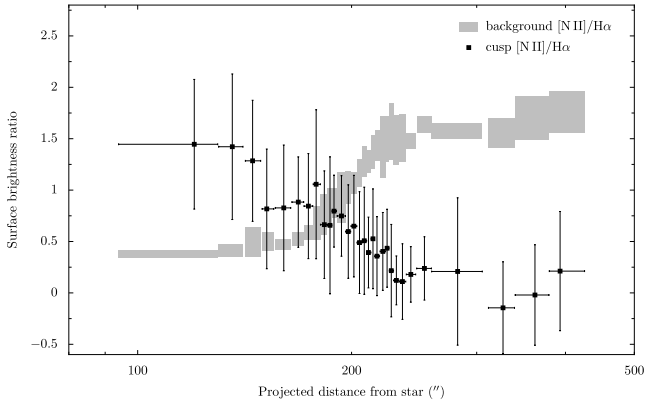


FIG. 7.—[N II]/H$\alpha$ ratio at the position of the knots.

of the bright cusps, but there is a weak correlation of increasing emission with decreasing projected distance from the central star.

The ratio of [N II] lines to the H$\alpha$ line cusp emission is shown in Figure 7. We see that [N II] becomes fainter relative to H$\alpha$ with increasing distance, whereas in the nebula the opposite is true. Each cusp is a microcosm of the nebula as a whole and should show all the ionization stages up to the highest stage seen in the local surrounding nebula. However, although the large-scale nebula is probably very close to photoionization equilibrium, the cusps themselves most certainly are not if they do indeed represent photoevaporation flows. This is because the dynamical time for the gas to flow away from the cusps is the same order as the photoionization timescale.

For gas in static photoionization equilibrium the ionization state at a given point is governed by the balance between recombinations and photoionizations according to the local electron density and radiation field, with the latter being strongly affected by the photoelectric absorption of H and He. For example, at larger radii in our observations the line of sight progressively becomes dominated by the helium neutral zone (from which [N II] emission primarily arises) as the ionization front of the inner disk and the outer ring is approached.

On the other hand, for very strongly advective flows, such as are found in the knot cusps, recombinations are unimportant, and the ionization state at a given point is given merely by the photoionization rate (cross section times ionizing flux) and the length of time since the gas was first exposed to ionizing radiation. Furthermore, the effective extreme ultraviolet optical depth to the ionization front is low (of order unity), so that radiative transfer effects are relatively unimportant, except at low ionization fractions. The simplicity thus gained, however, is offset by the complication that the ionization state is now intricately linked to the gas dynamics. One will still find an ionization stratification, but, since the cause is now different, one may see a difference in the detailed distribution of the ions.

The thermal balance in the ionized gas is also affected by the advection, since "adiabatic" cooling due to the gas acceleration and expansion can become comparable to the atomic cooling. The relative importance of advection in the cusps is expected to increase as the ionizing flux decreases, so knots that are farther away from the star might show lower temperatures in their photoevaporation flows. This is one possible explanation for the reduction in the [N II]/H$\alpha$ ratio with distance, which is explored more fully in § 4.2 below.

Knots in PNs are almost unique in their exemplification of this extreme regime of photoevaporation flows (Henney 2001).

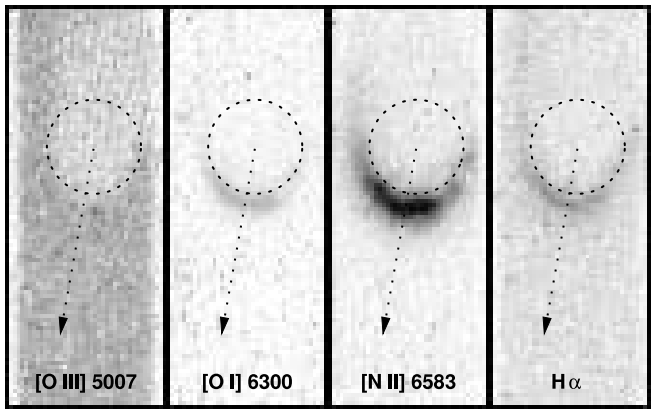


FIG. 8.—Composite images for various key ions in our analysis. They were formed by adding the appropriately scaled images of forbidden line doublets, and the H$\alpha$ image was corrected for the slightly overlapping [N II] $\lambda$6548 line's image. The circle identifies the knot core and is in the same location in each panel. The arrow indicates the direction toward the central star. [*See the electronic edition of the Journal for a color version of this figure*.]

H II regions are generally in the opposite "recombination-dominated" regime, where the effects of advection are considerably subtler (Henney et al. 2005b). The Helix knots are therefore an important laboratory for testing our understanding of the physics of this regime.

### 3.2. *Analysis of the STIS Slitless Spectrum Images*

As described in § 2.1, the slitless images were made at three grating settings. In several cases these included line doublets ([O I] $\lambda\lambda$6300, 6364, [N II] $\lambda\lambda$6583, 6548, and [O III] $\lambda\lambda$5007, 4959). Since each of these doublets arises from the same upper levels, the ratio of intensity of the components is constant and in each case close to 3:1. This means that we were able to derive higher quality images characteristic of each ion by combining the separate images of lines, a possibility exploited further by the fact that the [O I] lines appear at two grating settings, with the result that images of four lines are available. The H$\alpha$ + [N II] image is similar to that shown in Figure 1 of OHB00 in that the shorter wavelength [N II] line image slightly overlaps H$\alpha$. We circumvented this problem by scaling, shifting, and subtracting the image of the clearly separated longer [N II] line. The results are shown in Figure 8. We see that the [N II] emission is predominantly outside of the reference circle centered on the knot, whereas the [O I] emission peaks at roughly the same position as H$\alpha$. The radii and FWHM of the peak of the cusp emission are 0.″52 and 0.″21 for [O I], 0.″58 and 0.″30 for [N II], and 0.″54 and 0.″20 for H$\alpha$.

A more thorough presentation of the characteristics of the cusp is shown in Figure 9. In this figure we show the profiles of each of the ions, now including [O III], for all the data within 30° of the direction to the central star. The different cusp widths and locations of their peaks are well illustrated. It is obvious that the progression is not that expected from a simple ionization front, where the [O I] emission would be much narrower and clearly displaced toward the knot center, the [N II] emission would be farther out and only slightly wider, and the H$\alpha$ emission would be broadest and peak farthest from the knot center.

The explanation for this anomalous progression probably lies in the strong departures from static photoionization and thermal equilibrium in the cusps, as discussed in § 3.1. OHB00 could successfully reproduce the distribution seen in earlier observations by assuming a gradual rise in temperature of the gas as it

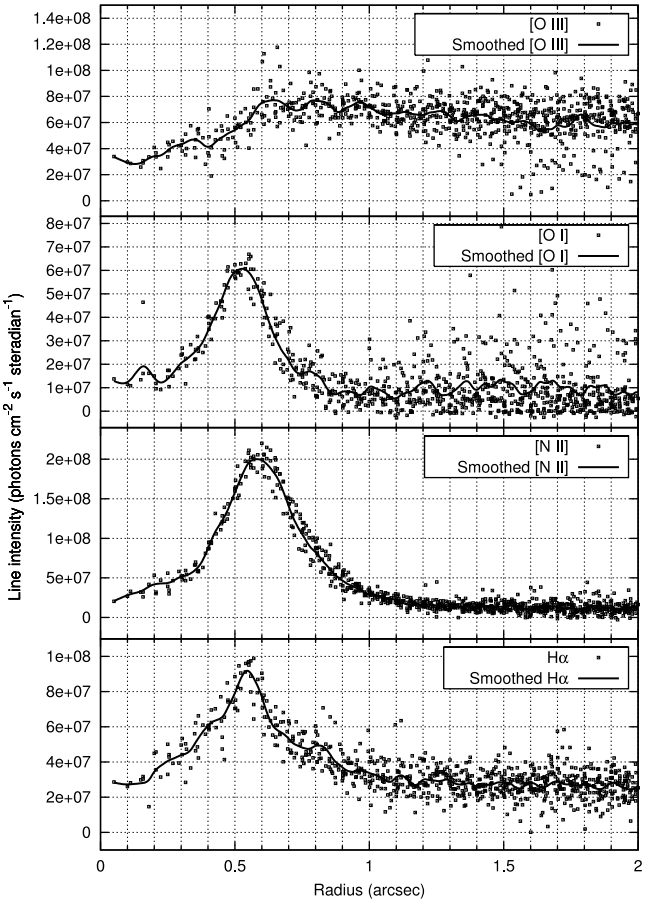


FIG. 9.—Radial profiles of emission-line surface brightness images of knot 378-801 as measured from the nominal knot center. Squares show all pixels whose radius from the knot center makes an angle $\theta < 30°$ with respect to the direction to the central star. A thick solid line shows a smoothed version of the same data.

becomes ionized. This is in contradiction to the usual structure of an ionization front, in which the gas temperature rises close to its equilibrium ionized value ($\sim 10^4$ K) *before* the gas becomes significantly ionized (Henney et al. 2005b). The OHB00 model is unsatisfactory in that the temperature structure was imposed in a totally ad hoc manner. This is rectified in § 4.2 below, where we present self-consistent radiation hydrodynamic models of the flows from the cusps.

### 3.3. *Analysis of the NIC3* $H_2$ *Images*

The best resolution ground-based study of $H_2$ in the entire Helix Nebula is that of S02, who imaged the entire nebula. Although their angular resolution is not stated, the pixel size employed was 2″, and the astronomical seeing was probably no worse than that, which means their effective resolution is comparable to the degraded focus FWHM of this study. Their image shows a few bright features within our NIC3 field, but our images go fainter than their limit and show many more knotty structures. Except for the east-west feature in the upper central portion of the left panel of Figure 4, there are no other features that correlate with the ground-based image.

In our images there is no indication of the cusp structure seen in the optical emission lines, which all arise from photoionized gas, but there are numerous emitting knots with a characteristic FWHM of 2.″3. In no cases do we see the central dips characteristic of the defocused star images, which means that the intrinsic

sizes of the $H_2$ cores are larger than a few pixels (about 0.″5). A Gaussian subtraction of the stellar FWHM (1.″8) from the average knot FWHM (2.″3) indicates an $H_2$-emitting core of FWHM = 1.″4, which is comparable to the size of the cores of the knots as outlined by extinction in [O III]. We do not see an elongation of the knots along a direction perpendicular to a line directed toward the central star, which is what we would expect if this emission came from a cusp-shaped form. However, the theoretical expectation is that the $H_2$ emission should come from a cusp-shaped $H_2$ zone lying between the emission-line cusp and the central core of the knot. These cusps would have to have elongations almost equal to the instrumental FWHM in order for us to see them. When we do see evidence of cusp structures, they are always large and knotty and have random orientations, indicating that they are chance superpositions of individual $H_2$-emitting knots.

An examination of F212N images of a southeast outer ring section of the Helix Nebula, made as part of program GO-9700, is useful. These images are in good focus, with stellar images of FWHM = 0.″3; however, the exposures showing knots were only 384 s in duration, and a thorough discussion of those images is not made here. The $H_2$ emission appears as cusps of the same form as those seen in ionization in the inner nebula. These cusps are about 0.″4 thick and 1.″8 wide. As noted in the previous paragraph, this type of image would not produce any noticeable elongation of our reduced-resolution images.

The images show that the brightest knots in our NIC3 field have values of $4\times10^{-5}$ ergs s$^{-1}$ cm$^{-2}$ sr$^{-1}$, which is much less than the values for the same region of greater than $10^{-4}$ ergs s$^{-1}$ cm$^{-2}$ sr$^{-1}$ indicated in Figure 6 of S02. The instrumental broadening of both sets of data could mean that the intrinsic surface brightness of the knots is higher than we give, but the comparable spatial resolution of both means that this cannot be the explanation of the differences between them. S02 does not report that any correction was made for continuum radiation in their $H_2$ filter, which could indicate that the overestimate could be due to underlying continuum. In our filter system the signal from the F212N filter was about 80% due to continuum, as determined from the F215N filter. S02 did not detect the Br$\gamma$ line at 2.166 $\mu$m, with an upper limit of $7\times10^{-8}$ ergs s$^{-1}$ cm$^{-2}$ sr$^{-1}$, which means that it is not a source of contamination of the F215N filter that we have used as a continuum reference.

We can approximately correct our peak surface brightness values using the information from the GO-9700 images. If the cusps have a rectangular size of 0.″4 × 1.″8 and our circular images have a diameter of 2.″3, then the scaling factor from our observed peak surface brightness to the intrinsic peak surface brightness will be $\pi1.15^2/0.4\times1.8 = 5.8$. This means that the observed peak surface brightness in our images ($4\times10^{-5}$ ergs s$^{-1}$ cm$^{-2}$ sr$^{-1}$) would have intrinsic (corrected) values of $2.3\times10^{-4}$ ergs s$^{-1}$ cm$^{-2}$ sr$^{-1}$.

A comparison of the *HST* NIC3 $H_2$ image with the CTIO ground-based H$\alpha$ + [N II] image is made in Figure 4. In this figure we see that there is no obvious correlation of the ionized gas emission with the $H_2$ emission. This far out from the central star the radiation is dominated by low-ionization emission (O98; Henry et al. 1999), which would be [N II] in this case, and the surface brightness of the ionized cusps drops to well below what can be resolved against the nebular background (for reference, see the discussion in § 4.1).

## 4. DISCUSSION

In this section we present and discuss the interpretation of our observations. In order to make the best use of them, we have developed extensive theoretical models. The first combines radiation and hydrodynamic effects, in support of explaining the optical emission-line observations; the second is a static model of the molecular region, in support of explaining the $H_2$ observations. We combine our new observations, our new models, and existing infrared and radio observations to develop a comprehensive model of the knots in the Helix Nebula.

### 4.1. *A General Model for 378-801*

We probably know more about the object 378-801 than about any other knot in the Helix Nebula because of the wide variety of observations that have been made of it. The best optical image is that of OH96, where the knot is the central object in their Figure 3. That source was used for preparing the monochromatic images shown in our Figure 10. The bright cusp is well defined in H$\alpha$ and [N II] with a central extinction core visible in [O III] emission. The tail is well defined with nearly parallel borders. At 8.″5 away from the bright cusp there is a secondary feature that starts on the east side of the tail and extends away from the central star without the bright cusp-form characteristic of other knots found this close to the central star. Its shape indicates that this is not a feature of the tail of 378-801; rather, it is a second knot that lies nearly along the same radial line from the central star.

#### 4.1.1. *The Core*

A molecular core in the knots was predicted by Dyson et al. (1989) before observational measurement and since then has been detected with increasing spatial resolution. The object 378-801 has been imaged in the CO $J = 1$–0 2.6 mm line by H02 with an elliptical Gaussian beam of 7.″9 × 3.″8 having an orientation of the long axis of P.A. = 14°, that is, at 18° from the orientation axis of the object. In that image one sees two peaks of CO emission, one on-axis 3″ from the bright cusp and a second associated with the overlapping feature, with a peak at 8″ from the bright cusp. Since they used the lower spatial resolution ground-based images of M92 for reference, they interpreted this feature as part of 378-801's tail, which it clearly is not. They also observed the object in the $H_2$ 2.12 $\mu$m line under conditions of seeing of 1.″2 and found a slightly broadened source just inside the curved optical bright cusp with a surface brightness of about $10^{-4}$ ergs s$^{-1}$ cm$^{-2}$ sr$^{-1}$ (using the S02 images for calibration). This image is consistent with the small cusps one sees in the southwest region of the Helix imaged in $H_2$ as part of program GO-9700 (§ 3.3). The CO source in the tail of 378-801 has a peak emission at $V_\odot = 31$ km s$^{-1}$ (H02 give $V_\odot = V_{\rm LSR} - 2.9$ km s$^{-1}$, and they work in LSR velocities). This velocity agrees well with $V_\odot = 31.6 \pm 1$ km s$^{-1}$ derived from optical spectra by M98, which means that there is not a large relative velocity of the CO source within the tail and its associated knot.

The distribution of dust within 378-801 is best determined by tracking the extinction of background nebular emission in the light of [O III], since the knot has little intrinsic [O III] emission. Figure 11 shows a trace of the surface brightness along the symmetry axis of the knot and its tail after normalizing the local background to unity. The maximum extinction gives a contrast of 0.5, which corresponds to an optical depth of 0.69. This value will be a lower limit if the knot does not lie in front of all the nebular [O III] emission. That seems to be the case, as M98 give high-resolution spectroscopic evidence (their § 5.1) that the knot is causing extinction only in the redshifted component of the nebula's light. This value of the optical depth is probably underestimated, since the nebular light will slightly fill in the

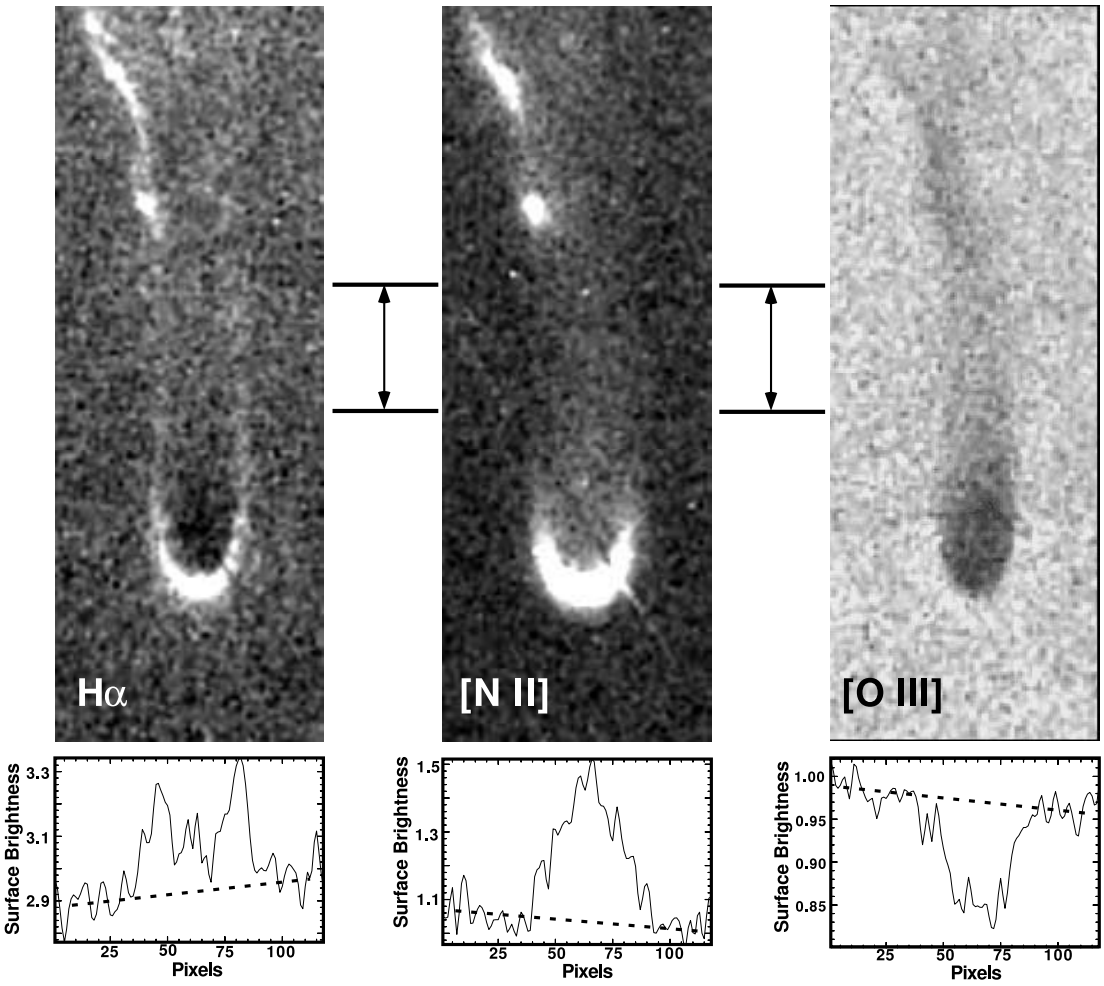


FIG. 10.—*Top panels*: From the WFPC2 programs GTO-5086 and GO-5311, 5.″9×16.″2 samples around 378-801 selected to lie along the symmetry axis of the tail, which coincides with a radial line drawn toward the central star. The pixel scale has been adjusted to 0.″05 in order to agree with that of the STIS images. The diagonal feature across the [N II] cusp is an artifact in the original image. The feature in the upper left portion of the Hα and [N II] images is probably a partially shadowed second knot that is unrelated to 378-801. The bands between the panels show the range of rows that were averaged when making the tail profiles (*bottom panels*). The limb brightening seen in Hα contrasts with the concentrated emission seen in [N II] and the concentrated extinction seen in [O III].

central region because of the finite point-spread function of the WFPC2 (McCaughrean & O'Dell 1996). Using the method of determination adopted by OH96 (which is similar to that of M92) and a gas-to-dust mass ratio of 150 (Sodroski et al. 1994) gives a lower limit to the mass within the entire core (a sample of 2.″1 × 2.″3 centered on the core) of $3.8\times10^{-5}\ M_{\odot}$. This is similar to the lower limit of $1\times10^{-5}\ M_{\odot}$ found from the CO observations for 378-801 and its nearby trailing feature (H02). The peak extinction corresponds to a lower limit of the column density of hydrogen of $1.7\times10^{21}$ hydrogen atoms $cm^{-2}$. If this material is concentrated to a distance corresponding to 1″, then the central hydrogen density of the knot is at least $5.2\times10^{5}\ cm^{-3}$.

As shown in § 3.2, the appearance of $H_2$ emission in a cusp just behind the ionized cusp is what is expected for a progression of conditions going from the outer ionized gas, through atomic neutral hydrogen, then into $H_2$. The innermost region of the core would be coldest and have the most complex molecules.

#### 4.1.2. *The Tail*

The appearance of the tail is a combination of the properties of the gas and dust found there and the photoionization conditions. A longitudinal scan of the cusp and tail in [O III] is shown in Figure 11, and a cross-sectional profile of a section of the tail is shown for Hα, [N II], and [O III] in Figure 10. Taking the [O III] extinction as a measure of the total column density and assuming axial symmetry, it appears that the tail is a centrally compressed column of material that decreases slowly in density with increasing distance from the center of the knot. The cause of this distribution is unknown, although it is consistent with the acceleration of the neutral gas via the rocket effect (e.g., Mellema et al. 1998). The low relative velocity of the core and the CO peak in the tail (§ 4.1.1) argue that this reflects the initial distribution of material following the formation of the core through an instability followed by radiation sculpting of the tail (O02).

Within the LyC shadow of the core the conditions will be very different from those in the nebula. This condition has been theoretically modeled by Cantó et al. (1998), and those models have been compared with observations of the knots in the Helix Nebula and the proplyds in the Orion Nebula (O'Dell 2000). Material in the shadow will only be illuminated by diffuse photons of recombining hydrogen and helium, with the most important being hydrogen. Because most of these recombinations will produce photons only slightly more energetic than the ionization threshold of hydrogen, whereas the stellar continuum is emitted mostly at higher energies, the average energy per

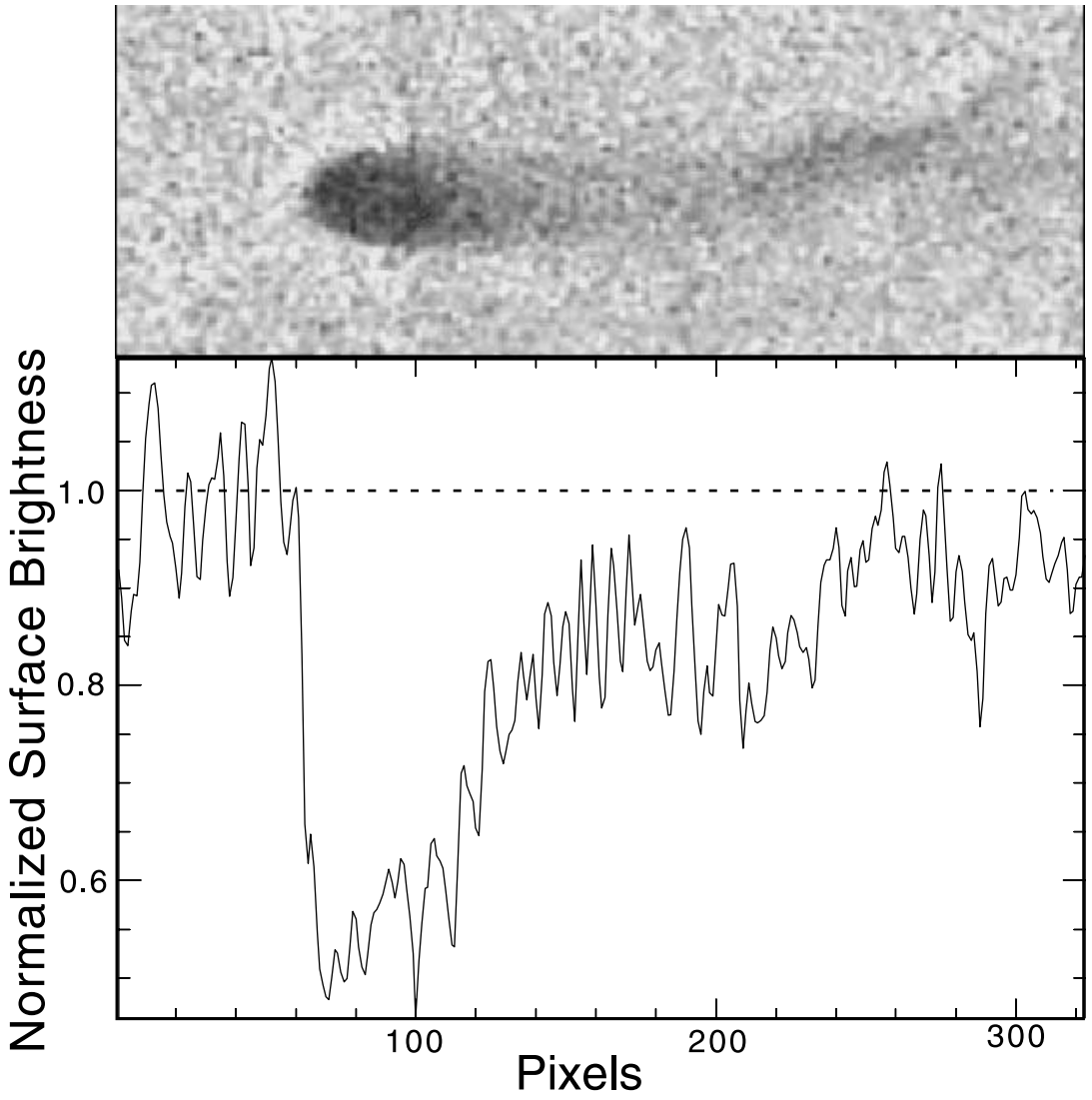


FIG. 11.—*Top*: Same as the [O III] image in Fig. 10. *Bottom*: Trace 0″.15 wide along the symmetry axis of the cusp and tail. This illustrates not only the concentration of extinction at the core of the knot, but that there is material that extends out to where the adjacent source confuses matters at about pixel number 200.

photon given to the gas in the shadow will be much lower than that in the nebula, and the electron temperature will be about two-thirds that of the nebula (Cantó et al. 1998; Osterbrock 1989). If the gas density within the shadow is sufficiently high, then there will be an ionization progression much like when one approaches the ionization front of an H II region, with a neutral core in the middle. If the gas density is low, then complete ionization of the shadow region will occur.

Our profiles in H$\alpha$ and [N II] across the tail shown in Figure 10 are very different. In H$\alpha$ we see strong limb brightening, as if we are seeing a cylinder of emission edge-on. In [N II] we see that the emission is very similar to that of the total column density of material, as measured by the [O III] extinction. The well-defined H$\alpha$ boundary makes it appear that only the outer part of the tail is photoionized. However, to create the collisionally excited [N II] lines, one needs both electrons of several electron volt energy and singly ionized nitrogen. It is obvious that a more sophisticated photoionization model is required, and the paper by Wood et al. (2004) is a step in this direction; however, it is not directly applicable to this knot, because they only consider a shadow formed in a region surrounded by only singly ionized helium.

### 4.2. *Models of the Knots That Combine Hydrodynamics and Radiation*

In order to model the properties of the ionized flows from the cometary knots, we have carried out a preliminary numerical study of the dynamical evolution of a dense neutral condensation, subject to the effects of stellar ionizing radiation. The simulations were carried out by means of the radiation hydrodynamics code described in Henney et al. (2005a). The initial conditions for the simulation were a cylindrical[4] concentration of dense neutral gas, with core radius $2\times10^{15}$ cm and density $3\times10^{4}$ cm$^{-3}$, which was illuminated by an ionizing spectrum similar to that of the Helix central star ($T_{\rm eff} = 120,000$ K; ionizing luminosity $Q_{\rm H} = 7.8\times10^{45}$ s$^{-1}$). The local diffuse field is treated in the on-the-spot approximation, and the global nebular diffuse field, with an expected strength of only 1%–4% of the direct radiation (López-Martín et al. 2001), is neglected. The only source of opacity considered in the simulations is

[4] Although the initial shape of the globule may affect its subsequent evolution and eventual destruction, the properties of the ionized flow from the globule head should be insensitive to this.

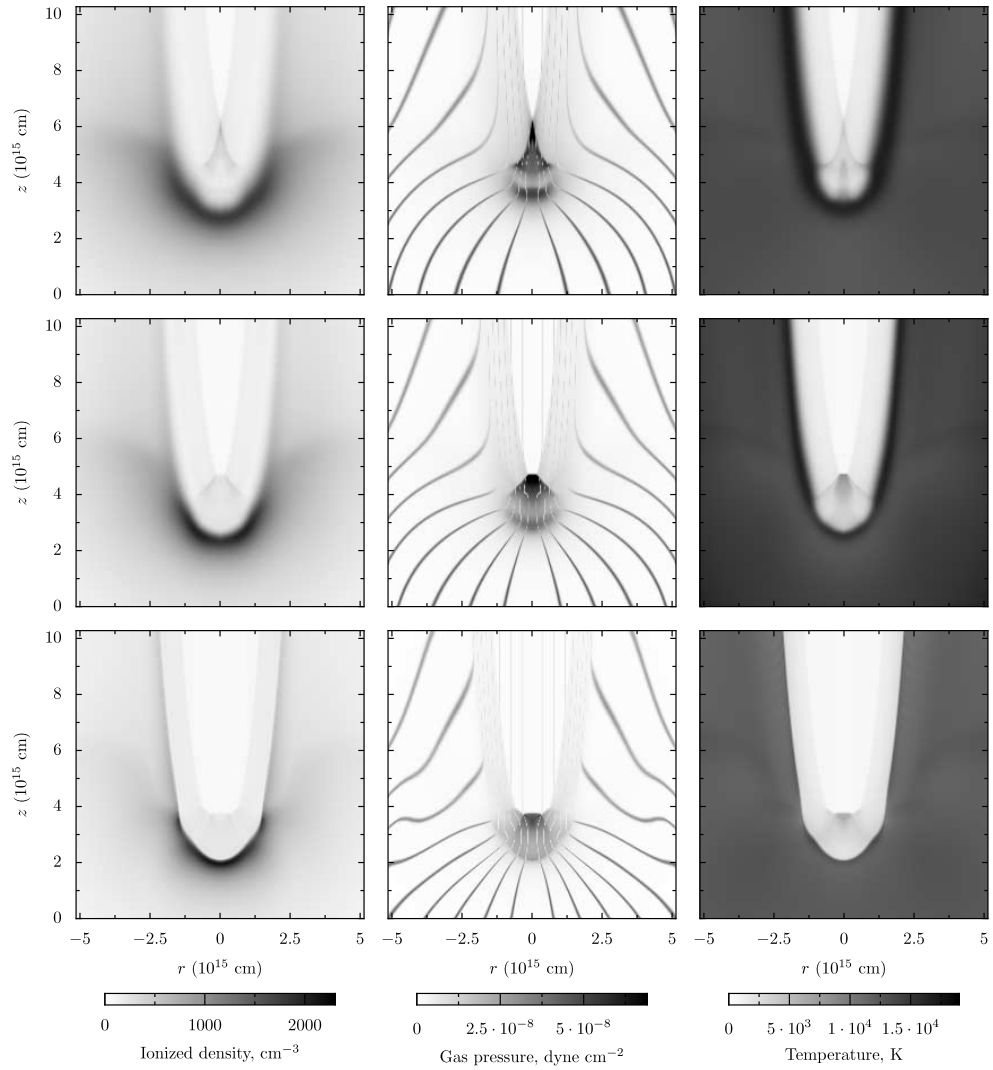


FIG. 12.—Physical structure of the model simulations at an age of 132 yr for a knot at a distance of $4.63\times10^{17}$ cm from the ionizing star. The three rows show simulations calculated using different degrees of hardening for the ionizing radiation (most hardening in the top row, no hardening in the bottom row). The three columns show ionized gas density, gas pressure, and gas temperature (*left to right*). The middle column also shows contours of the initial cylindrical radius of the gas at each point, which serve as approximate streamlines for the ionized part of the flow.

photoelectric absorption. (The dust optical depth through the ionized flow in the ionizing ultraviolet is only of order 0.01 and can be safely neglected.) Free expansion conditions were used on the grid boundaries, which is reasonable since the ionized flow becomes supersonic. A simple ram pressure balance argument indicates that the standoff shock between the ionized globule flow and the ambient nebular gas should occur at about 50 times the globule radius, which is outside our computational grid. Any wind that may exist from the central star is confined very close to the center of the nebula (Zhang et al. 1993) and does not affect the knots.

Models were run with the globule located at various distances from the star between $3\times10^{17}$ and $10^{18}$ cm, and the evolution was followed for approximately 500 yr. A snapshot of the structure of a typical model is shown in Figure 12.

The photoevaporation of the surface layers drives a shock wave through the knot, which compresses it and accelerates it away from the ionizing star (Bertoldi 1989; Mellema et al. 1998; Lim & Mellema 2003). In our simulations, the neutral clump reaches speeds of order 2–5 km $s^{-1}$. At the same time, an ionized photoevaporation flow develops from the head of the clump, which accelerates back toward the star, eventually reaching speeds of order 20 km $s^{-1}$. The bulk of the optical line emission is produced by denser, slower moving gas from the base of the photoevaporation flow, near the ionization front, as can be seen in Figure 12 (*left panels*), which shows the ionized gas density. Three models are shown that differ in their treatment of the hardening of the radiation field, which is treated only very approximately in the current simulations. In the model with maximum hardening (*top panels*), the ionization front is very broad and the gas temperature (*right panels*) has a pronounced maximum on the neutral side of the front. When the hardening is reduced (*bottom panels*), the front is much sharper, with a less pronounced temperature peak. The pressure of the photoionized flow (*middle column*) is also higher in the models with greater hardening, and, as a result, a stronger shock is driven into the neutral knot. Weaker shocks, which eventually converge and bounce off the symmetry axis, are also driven in from the flow from the sides of the knot, as in Figure 12 (*top panels*).

Although these two-dimensional simulations do not contain all the details of atomic physics that have been included in

one-dimensional models (e.g., Henney et al. 2005b), they nonetheless capture the most important physics of the photoionized flow, which is dominated by photoelectric heating and expansion cooling, and therefore they can provide a tool for investigating the physical basis of the observed optical emission properties of the knots. The most important of these are that the [N II]/H$\alpha$ ratio falls precipitously with distance of the knot from the central star (§ 3.1) and that the [N II] emission from the best-studied individual cusps is found to lie slightly outside the H$\alpha$ emission (§ 3.2). OHB00 attempted to explain the second of these by positing an ad hoc broad temperature gradient in the photoevaporation flow, leading to enhanced collisional line emissivity and depressed recombination line emissivity at greater distances from the knot center.

We have calculated for each model the emission properties of the cusps as follows. First, we automatically identified the ridge in the ionized density at the cusp and fitted for its curvature. Using the position and curvature of the cusp we determined a nominal center for the knot. Then we derived radial emissivity profiles as a function of distance from the knot center, averaging over all radii within 60° of the symmetry axis. From these profiles, we calculated the mean surface brightness of the cusp and its mean radius from the knot center for each emission line. These steps were carried out for each of a sequence of times in the evolution of the knot up to an age of $\simeq$500 yr and were averaged to give a global mean and standard deviation for each model.[5] In the final averaging the initial 50 yr of evolution were omitted, since this represents a highly nonsteady phase in which the flow is still adjusting to its quasi-stationary configuration.

The lines that we considered were H$\alpha$ and [N II] $\lambda$6583, with temperature-dependent emission coefficients that were calibrated using the CLOUDY plasma code (Ferland 2000). The ionization fraction of nitrogen was assumed to exactly follow that of hydrogen, and double ionization of nitrogen was neglected. (The extreme weakness or absence of [O III] emission from the cusps indicates that this is a reasonable approximation.)

The results are shown in Figures 13 and 14 for two different sets of models, which differ in their treatment of the hardening of the radiation field and in the contribution of helium to the photoelectric heating. Figure 13 (*top*) shows that the mean radius of the [N II] emission is indeed larger than that of H$\alpha$, but only significantly so for knots that are farther than 200″ from the central star. This is a direct result of the temperature structure in the ionized flow, which has a maximum close to the peak in the ionized density. For the farther knots, this temperature peak is slightly outside the ionized density peak, which biases the [N II] emissivity to larger radii.

Figure 14 (*top*) shows that the [N II]/H$\alpha$ surface brightness ratio of the knots does decline with distance, particularly for the model with less hardening. This is a direct result of the flow not attaining such high temperatures when the knot is farther from the star, which is due to the increased relative importance of "adiabatic" cooling as the flow accelerates. However, although this behavior is in qualitative agreement with the observations, the decrease seen in the models is much less sharp than that seen in the real nebula. It should also be noted that we have had to assume a nitrogen abundance of N/H = $1.2\times10^{-4}$ in order for the absolute values of our [N II]/H$\alpha$ ratio to be consistent with the observations. This is roughly 2 times lower than the abundance that has previously been derived for the nebula as a whole (Henry et al. 1999).

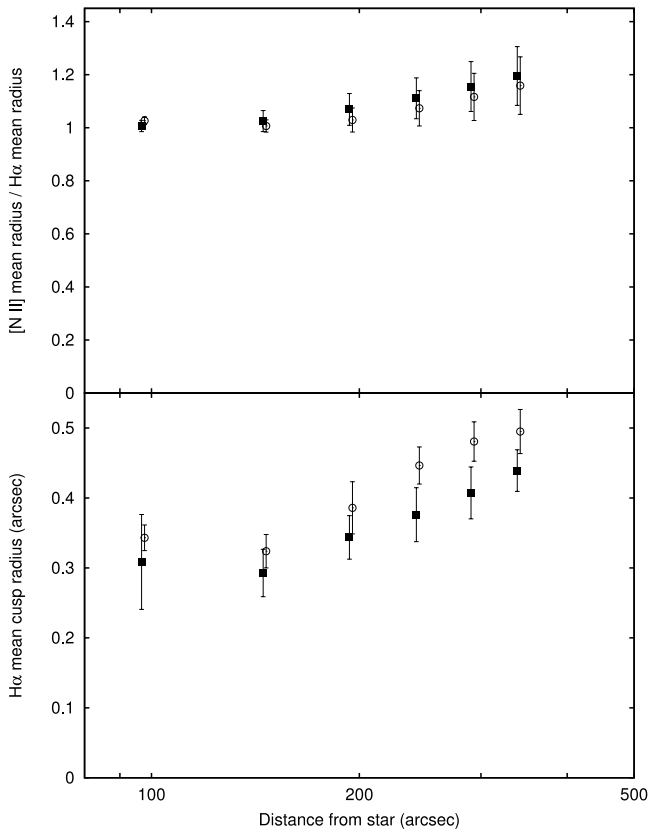


FIG. 13.—Model predictions for knot cusp radius as a function of distance from the central star. *Bottom*: Mean radius of H$\alpha$ emission from the cusp in arcseconds. *Top*: Ratio of mean cusp radius in [N II] to that in H$\alpha$. Vertical bars indicate the range of values during the evolution of the models. Different symbol types correspond to models with differing treatment of the radiation hardening and photoelectric heating (see text).

The N abundance that we find from our models is close to the solar value and is very similar for the models with different hardening. Although this could be interpreted as evidence for differing abundances between the knots and the rest of the ejecta, we do not think that such an inference is warranted. The photoionization models on which previous abundance studies have been based are only very crude representations of the three-dimensional structure of the nebula, so their derived abundances are probably not reliable.

Figure 14 (*bottom*) shows the dependence on distance of the H$\alpha$ cusp surface brightness of the models. The values shown are for a face-on viewing angle and thus should be multiplied by a factor of a few to account for limb brightening. Once this is taken into account, the predictions are in very good agreement with the observed values (Fig. 5) and in particular fall well below the line derived from equating recombinations in the flow to the incident ionizing flux, which is an illustration of the importance of the advection of neutrals through the front, as discussed in López-Martín et al. (2001).

It is heartening that our simple radiation hydrodynamic models are qualitatively consistent with the trends seen in the observations, although there are some quantitative discrepancies. In particular, in the models, both the reduction in the knot [N II]/H$\alpha$ surface brightness ratio and the increase in the size of

[5] In order to explore the mechanism of formation and evolution of the knots, it would be desirable to perform fuller simulations that tracked the knots over thousands of years. However, our present simulations have only the more limited goal of explaining the properties of the ionized flow. For this purpose, we feel that the baseline of 500 yr, which represents about 15 dynamic times for the ionized flow, is sufficient.

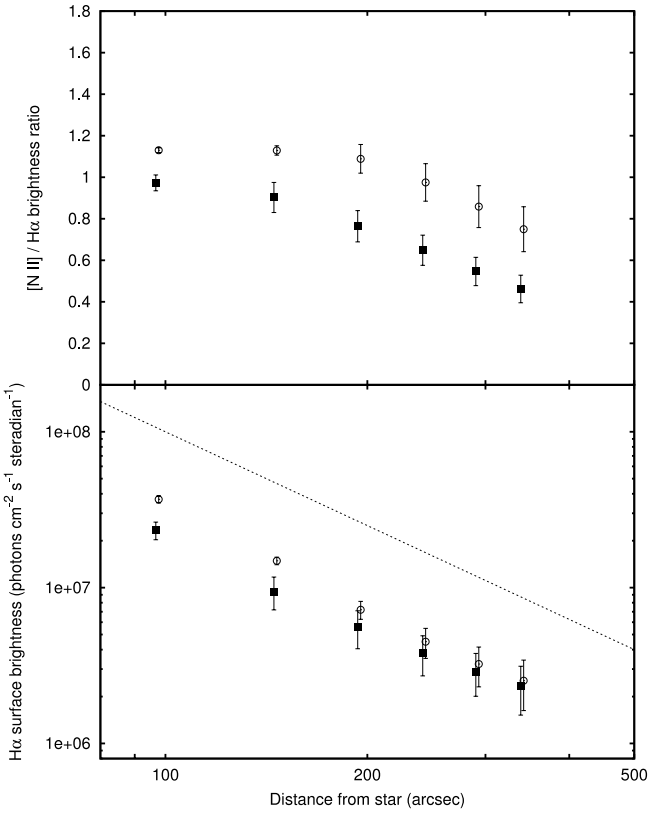


FIG. 14.—Model predictions for knot surface brightness as a function of distance from the central star. *Bottom*: Face-on surface brightness of H$\alpha$ emission from the cusp. The dotted line shows the simplistic prediction, as in Fig. 5. *Top*: Ratio of [N II] surface brightness to that of H$\alpha$. Symbol types are the same as in Fig. 13.

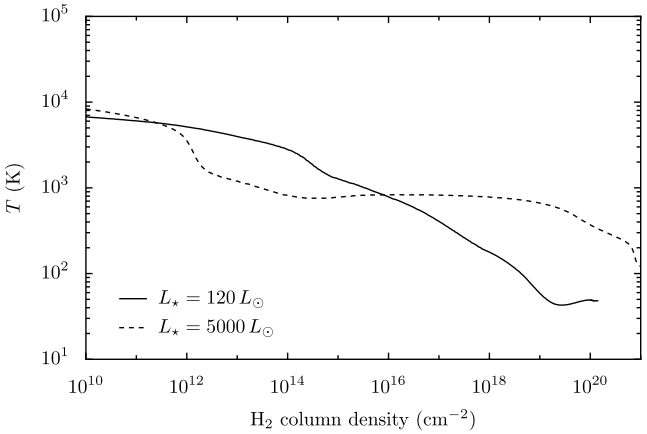


FIG. 15.—Gas temperature as a function of molecular hydrogen column density for our CLOUDY models of the knot PDR. The solid line shows a model calculated using our best estimates of parameters appropriate for the Helix knots. The dashed line shows the $t = 4000$ yr case considered by NH98. The largest difference is that the central star luminosity is about a factor of 40 larger. Grain photoelectric heating of neutral gas creates a significant warm (about 900 K) region.

the [N II] cusp relative to the H$\alpha$ cusp only occur at large distances from the central star, whereas in the Helix they are observed to occur at smaller distances. Although this may be in part a projection effect, due to the projected distances of the knots being smaller than their true distances, that is unlikely to be the whole explanation. One possibility is that the farther knots see a much-reduced ionizing flux due to recombinations in the nebula between them and the ionizing star, whereas in our models we assume only a geometric dilution of $1/r^2$.

It is also possible that some of the atomic physics processes that have been neglected in our models may prove important in determining the thermal structure. More realistic simulations are in preparation, and it remains to be seen whether they will lead to an improvement in the agreement with observations.

### 4.3. $H_2$ *Emission*

In addition to the surface brightness in the $H_2$ 2.12 $\mu$m line discussed in § 3.3, there is the important and constraining result of Cox et al. (1998), who determined from *Infrared Space Observatory* spectrophotometry of six $H_2$ lines that this gas has an excitation temperature of 900 K. In this section we show that radiation-only heating models cannot explain such a high temperature.

The other basic constraint is the column density of $H_2$. If the molecular gas is in LTE, then the surface brightness in an optically thin line is simply related to the gas column density. We adopt a 2.12 $\mu$m $H_2$ line surface brightness of $2.3\times10^{-4}$ ergs cm$^{-2}$ s$^{-1}$ sr$^{-1}$. At 900 K, we expect

$$S(H_2;\ 2.12\ \mu\mathrm{m}) = 3.83\times10^{-24} N(H_2)\ \mathrm{ergs\ cm^{-2}\ s^{-1}\ sr^{-1}}$$

and obtain a column density of $N(H_2) \simeq 6\times10^{19}$ cm$^{-2}$, or $N(H) \simeq 12\times10^{19}$ cm$^{-2}$ if the gas is fully molecular. This warm $H_2$ layer has a physical thickness of $1.2\times10^{15}$ cm (§ 3.3), so we find a density of $n(H_2) = N(H_2)/\delta r \simeq 6\times10^4$ cm$^{-3}$. This is not significantly smaller than the density Cox et al. (1998) quote for $H_2$ to be in LTE. We assume this density in the remaining work.

Since the emissivity is driven by the excitation temperature, the cause of the high temperature must be resolved prior to comparing the observed and predicted surface brightness of the $H_2$ 2.12 $\mu$m line. We present our model in § 4.3.1, give an interpretation of the observations and derive the additional heating required in § 4.3.2, and discuss other relevant observations of the core of the knots in § 4.3.3. A critique of previous comparisons of $H_2$ observations and models is presented in § 4.3.4.

#### 4.3.1. *The Predicted Knot* $H_2$ *Properties*

For simplicity, we assume that the knot is illuminated by the full radiation field of the central star—a good assumption, since the nebula is quite optically thin up to where knots are first detected. We assume a separation from the central star of 0.137 pc, appropriate for the knot 378-801. We further assume that the knot has the same gas-phase abundances as the H II region (Henry et al. 1999). The illumination is assumed to be from a blackbody of 120,000 K and 120 $L_\odot$ (Bohlin et al. 1982, adjusted to a distance of 213 pc). In addition, we assume an ISM dust-to-gas ratio and grain size distribution but do not include polycyclic aromatic hydrocarbons (PAHs), since Cox et al. (1998) report that no PAH emission is seen. We assume that the density is constant across the knot in our photodissociation calculations. Cox et al. (1998) convincingly argue that the lower levels of $H_2$ are in LTE and that this requires a density $n \geq 10^5$ cm$^{-3}$, which is much higher than the characteristic density (1200 cm$^{-3}$) in the ionized zone (OB97).

With these assumptions the conditions within the knot can be calculated with no unconstrained free parameters. The solid line in Figure 15 shows the gas temperature as a function of the column density of molecular hydrogen as one goes into the knot. It can be seen that the column of warm $H_2$ is very low (about $10^{16}$ cm$^{-2}$ for $T > 900$ K) and that the temperature has fallen to about 50 K before an appreciable column density is reached, much lower than the observed $H_2$ temperatures.

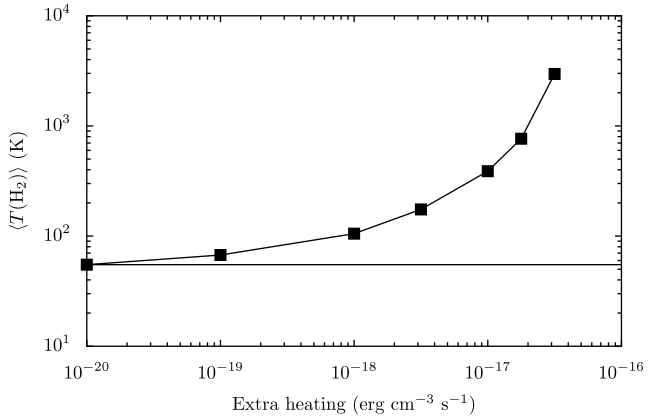


FIG. 16.—Enhancement of the temperature of the gas in our model knots as a function of the added extra heating. The horizontal solid line shows the expected value with no extra heating.

This result seems to conflict with Natta & Hollenbach (1998, hereafter NH98), who found significant amounts of warm (900 K) molecular gas in their model for a PN envelope at an evolutionary age of 4000 yr. We recomputed this case using the time-steady assumption and approximating the dynamics with constant gas pressure. While the time-steady assumption is not really appropriate for the $H_2$ transition region because of the long formation timescales, it is valid for both the atomic and fully molecular regions and serves to illustrate the important physics. The dashed line in Figure 15 shows this calculation. While we do not reproduce their large region of hot ($10^4$ K), predominantly atomic H, we see the essential features of the transition and fully molecular regions. In particular, a significant amount of gas has a temperature of about 900 K. This is due to grain photoelectric heating of the gas, as NH98 point out. Although this process does occur in our fiducial Helix model, it is not able to sustain warm temperatures, mainly because of the much lower luminosity of the Helix central star. The cooling time in the molecular gas is very short (of the order of decades), so time-dependent effects are unlikely to change this result. Indeed, NH98 find a similar behavior at later evolutionary times, after the luminosity of the central star has declined. For example, their model results at an age of 7000 yr no longer show a significant column of warm molecular gas.

In conclusion, it would be possible to achieve the derived column density of heated molecular hydrogen ($6\times10^{19}$) only by increasing the luminosity of the central star by more than an order of magnitude from the observed value. In the following section, we investigate the possibility that the warm $H_2$ may instead be heated by shocks.

#### 4.3.2. *Are Shocks the Source of the Warm* $H_2$*?*

In this section we derive the rate of extra heating that would be necessary to explain the 900 K temperature and assess whether this can be explained by shock heating.

As shown in § 4.3.1, the expected $H_2$ temperature is about 50 K for the conditions present in the Helix when only radiation from the central star and the X-ray source heat the gas. Something else, probably mechanical energy, must add heat to the molecular gas to obtain a temperature as high as 900 K. We quantify this by adding increasing amounts of extra heating to our fiducial model. The results are shown in Figure 16. The extra heating is shown along the *x*-axis, and the *y*-axis gives the $H_2$ weighted mean temperature. An extra heating rate of about $10^{-16.8}$ ergs cm$^{-3}$ s$^{-1}$ is necessary to account for the observed $H_2$ temperature. For comparison, the radiative heating across the $H_2$ region is $10^{-19}$ ergs cm$^{-3}$ s$^{-1}$. Since the warm $H_2$ extends over a physical thickness of $1.2\times10^{15}$ cm, the extra power entering the layer to sustain the heating over this thickness is $1.9\times10^{-2}$ ergs cm$^{-2}$ s$^{-1}$.

One source of nonradiative heating that naturally springs to mind is shock heating. For the shock hypothesis to be viable, three requirements must be satisfied:

1. The shock velocity should be just high enough to heat the gas up to 900 K and excite molecular hydrogen emission.
2. The rate of energy dissipated in the shock must be sufficient to provide a heating rate of $2\times10^{-17}$ ergs cm$^{-3}$ s$^{-1}$ in a layer of thickness $10^{15}$ cm.
3. In the case of a transient shock, the cooling time in the molecular gas must be sufficiently long that the gas remains hot for a significant time after the shock has passed.

For fully molecular conditions ($\gamma = 7/5$, $\mu \simeq 2.36$), the first requirement is satisfied for shock velocities in the range 4.5–5 km s$^{-1}$. The second requirement demands an energy flux through the shock of 0.02 ergs cm$^{-2}$ s$^{-1}$, which, combined with the first requirement, implies a preshock hydrogen nucleon density of $\simeq4.2\times10^4$ cm$^{-3}$ and a postshock density of $\simeq2.6\times10^5$ cm$^{-3}$. Within the margins of error, this density is consistent with the values discussed above. Our hydrodynamic models of § 4.2 show that several shocks of this approximate speed are indeed generated in the radiatively driven implosion of the knot.

However, the third requirement proves to be the most difficult to satisfy, even in its weakest form, which requires that the time taken for gas to pass through the thickness of the $H_2$ layer be less than the cooling time, $P/[(\gamma-1)L] \simeq 20$ yr (where $L$ is the volumetric cooling rate). This implies that the particle flux through the layer be larger than the column density divided by the cooling time, $nv \gtrsim 2\times10^6$ cm$^{-3}$ km s$^{-1}$. In our simulations we find particle fluxes that are at least 10 times smaller than this value. Furthermore, since the shock speed of $\simeq5$ km s$^{-1}$ exceeds the propagation speed of the ionization front at the knot's cusp, the shocks quickly propagate up the tail and away from the cusp. This is hard to reconcile with the observed location of the $H_2$ emission in 378-801 unless we are seeing this knot at a special time.

In summary, although shocks are initially attractive as a mechanism to explain the observed $H_2$ emission, they seem to be ruled out by cooling time arguments. The gas temperature is only enhanced in the region immediately behind the shock, which is difficult to reconcile with the observed location of the $H_2$ emission, which is immediately behind the cusp ionization front. This objection could be avoided if the shock were a stationary structure in the head of the knot, i.e., if the shock and cusp were propagating at the same speed. However, such a solution is very contrived, and no such stationary shocks are ever seen in our hydrodynamic simulations.[6]

#### 4.3.3. *A Summary of Properties of the Core of the Knots*

H02 have resolved the knot 378-801 in both $H_2$ and CO, finding that the $H_2$ emission is well displaced toward the bright optical cusp from the CO emission, which comes from the core

[6] In the case of the Orion proplyds, just such a stationary shock *is* found, driven by the back pressure of the ionization front acting on the neutral photoevaporative wind from the accretion disk (Johnstone et al. 1998). However, the Helix knots do not possess an ultradense reservoir of neutral gas such as is found in the proplyds.

of the knot. CO will only exist if $H_2$ is also present, since the chemistry that leads to CO is initiated by interactions involving $H_2$. This means that the core emission must come from a cooler, higher density region than the $H_2$ emission. The optical depth for CO to be formed is about $\tau \simeq 4$ (Tielens et al. 1993). If the optical depth is the factor determining the displacement of the peak of CO (about $3''.5 \simeq 10^{16}$ cm), then the intervening column of gas has a density of about $10^6$ cm$^{-3}$.

Dust extinction also provides an estimate of the total hydrogen column density through the center of the knot, presumably the core of the cool CO region. The observed extinction ($\tau \simeq 0.7$; OB97) corresponds to $N(\mathrm{H}) \simeq 1.7 \times 10^{21}$ cm$^{-2}$ for an ISM dust-to-gas ratio. This dust extinction occurs across a region of about $1''$ ($3 \times 10^{15}$ cm), so the density in the CO region is $n(\mathrm{H}) \simeq 6 \times 10^5$ cm$^{-3}$. The fact that the core extinction is less than that required to avoid photodissociation of CO argues that the core is unresolved on our *HST* images and that the larger ($10^6$ cm$^{-3}$) density applies. This larger density is an order of magnitude higher than our estimate of the density in the hot $H_2$ zone. Since the CO temperature is probably about that of our model without the extra heating, the hot $H_2$ zone and the core are about in pressure equilibrium.

#### 4.3.4. *Previous Comparisons of $S_{2.12\ \mu\mathrm{m}}$ with Evolutionary Models of Planetary Nebulae*

In a recent paper Speck et al. (2003, hereafter S03) present new images of NGC 6720 (the Ring Nebula) in $H_2$ 2.12 $\mu$m at an unprecedented resolution of $0''.65$. They find that the Ring Nebula resembles the Helix Nebula in $H_2$ in that the emission is concentrated into small knots, some of which were already known to have tails (O02), and these knots are arrayed in loops. It was already known (O02) that the Ring and Helix nebulae have similar three-dimensional structures and that the Ring Nebula is in an earlier stage of its evolution, with much more extinction in the tails outside of the knots. This last point argues that the tail material is residual material from the formation process, rather than being expelled from the knot.

S03 compare the average values of $S_{2.12\ \mu\mathrm{m}}$ for the Ring Nebula, the Helix Nebula, and NGC 2346 with the predictions of an evolutionary model for NGC 2346 derived by Vicini et al. (1999). In S03's Figure 3 they compare the average values of $S_{2.12\ \mu\mathrm{m}}$ with the predictions of the Vicini et al. models for various ages of the nebulae and argue for good agreement, even though the observed average surface brightness of the Helix Nebula is much larger than the predictions of the model, using their adopted age of 19,000 yr. If one uses the most recent determination of 6600 yr (OMM04), then the agreement becomes good for the Helix Nebula. However, if one uses S03's average surface brightness for NGC 6720 but the best value of the age of 1500 yr (O02), then that object is much too bright for its age.

We note that S03's Table 1 gives an average value of $S_{2.12\ \mu\mathrm{m}}$ for the Helix Nebula of $6 \times 10^{-5}$ ergs s$^{-1}$ cm$^{-2}$ sr$^{-1}$, whereas the source they cite (S02, § 2.3) gives an average value of $2 \times 10^{-4}$ ergs s$^{-1}$ cm$^{-2}$ sr$^{-1}$. The reason for this difference is that the earlier, larger value refers to the average surface brightness of individual knots, whereas the S03 value refers to an average surface brightness over an extended area (A. K. Speck 2005, private communication). The average brightness of the knots in S02 ($2 \times 10^{-4}$ ergs s$^{-1}$ cm$^{-2}$ sr$^{-1}$) is comparable to the value of $2.3 \times 10^{-4}$ ergs s$^{-1}$ cm$^{-2}$ sr$^{-1}$ that we derived in § 3.3 for the peak surface brightness of the knots.

There is reason to question acceptance of the procedure of comparison of the Vicini et al. (1999) model and the observed average surface brightnesses of the Ring and Helix nebulae. The Vicini et al. model draws on the general theory for an evolving PN published by NH98. In both the Ring Nebula (S03) and the Helix Nebula (S02) one sees that $H_2$ emission arises primarily from the knots, rather than from an extended PDR behind the main ionization front of the nebula. In their "Summary and Conclusions" section NH98 point out that knots do not adhere to their general model and would have a higher surface brightness. However, since the knots cover but a fraction of the image of the nebulae, the average surface brightness is lower than the value for the individual knots and depends on the angular filling factor. This means that one cannot compare the average surface brightness of a knot-dominated nebula with the predictions of a simple evolving nebula unless one has both a detailed model for the knots and an accurate determination of their angular filling factor.

### 4.4. *On the Association of the Knots and* CO *Sources*

There is reason to argue that all the measured CO sources seen in the Y99 study are associated with knots. As the spatial resolution of the CO observations has improved (Huggins & Healy 1986; Healy & Huggins 1990; Forveille & Huggins 1991; Huggins et al. 1992; Y99), there has been a progressive increase of ability to isolate individual knots; the best resolution study (H02) targeted and found the target knot of this study (378-801), as discussed in § 4.3.3. Even at the lower resolution of the Y99 study, spectra of individual data samples commonly show multiple peaks of emission at various nearby velocities, indicating that the unresolved regions are actually composed of multiple emitters. A similar progression of improved resolution in $H_2$ observations has produced clear evidence for association with knots (S02). The isolation of individual knots becomes more difficult as one goes farther from the central star, because the numerical surface density of knots increases rapidly and the lower resolution CO studies appear amorphous first, and the higher resolution $H_2$ studies only appear amorphous in the outermost regions.

Y99 point out that, dynamically, there appear to be two types of CO emitter. The first type is a group of small sources all found within $300''$ of the central star. The velocities of these sources are distributed as if they all belong to an expanding torus region, which produces a nearly sinusoidal variation in the radial velocities with an amplitude of $\pm 17$ km s$^{-1}$, as found earlier by Healy & Huggins (1990). Y99 call these sources the inner ring. The second type of emitter is found in the regions they call the outer arcs. The explanation for these two velocity systems was presented in OMM04, who demonstrated that these are knots associated with the outer parts of the inner disk and the outer ring, which have different expansion velocities and tilts with respect to the plane of the sky. The absence of CO emission from the PDRs surrounding the nebular ionization fronts is probably due to the fact that the optical depth in the photodissociating continuum does not become large enough to allow formation of CO. Certainly, there is no evidence for a large optical depth in the visual continuum on the outside of the nebula, as there is no obvious depletion of stars.

### 4.5. *Conclusions*

Our observations and models of the knots in the Helix Nebula have shown that these are objects strongly affected by the radiation field of the central star. The central densities of their cores are about $10^6$ cm$^{-3}$, with the side facing the star being photoionized. The peculiar surface brightness distribution of the [N II] and H$\alpha$ cusps is explained by the process of photoablation of material from the core. The knots are at the extreme of the

regime of photoevaporation flows in terms of the importance of advection. The $H_2$ emission arises from warm regions immediately behind the bright cusps, with a density of about $10^5$ cm$^{-3}$ and with a temperature that cannot be explained by radiative heating and cooling. The shadowed portions of the tails behind the cores are easily seen in CO because of the increased optical depth in the stellar continuum radiation. We point out that earlier calculations of conditions in the molecular zones around the PNs have temperatures that are too high, and that previous applications of these models to observations of other PNs were flawed.

We are grateful to Bruce Balick of the University of Washington and Arsen Hajian of the United States Naval Observatory for their participation in planning the observations reported on in this paper. We also thank Robin J. R. Williams for many helpful conversations. Our thanks also go to Angela K. Speck of the University of Missouri for clarification of the difference in meaning of the surface brightness values for NGC 7293 included in S02 and S03 and for discussions on comparison of the observed average $H_2$ surface brightness with the models of Vicini et al. (1999). C. R. O.'s work on this project was partially supported by STScI grant GO-9489. W. J. H. acknowledges financial support from DGAPA-UNAM, Mexico, through project PAPIIT-IN115202 and a sabbatical grant and is also grateful to the University of Leeds, UK, for hospitality during his sabbatical visit. G. J. F.'s work was supported in part by NASA NAG5-12020 and STScI AR 10316.

REFERENCES

Bertoldi, F. 1989, ApJ, 346, 735
Bohlin, R. C., Harrington, J. P., & Stecher, T. P. 1982, ApJ, 252, 635
Cantó, J., Raga, A., Steffen, W., & Shapiro, P. R. 1998, ApJ, 502, 695
Capriotti, E. R. 1973, ApJ, 179, 495
Cerruti-Sola, M., & Perinotto, M. 1985, ApJ, 291, 237
Cox, P., et al. 1998, ApJ, 495, L23
Dyson, J. E., Hartquist, T. W., & Biro, S. 1993, MNRAS, 261, 430
Dyson, J. E., Hartquist, T. W., Pettini, M., & Smith, L. J. 1989, MNRAS, 241, 625
Ferland, G. J. 2000, Rev. Mex. AA Ser. Conf., 9, 153
Forveille, T., & Huggins, P. J. 1991, A&A, 248, 599
Harris, H. C., Dahn, C. C., Monet, D. G., & Pier, J. R. 1997, in IAU Symp. 180, Planetary Nebulae, ed. H. J. Habing & H. J. G. L. M. Lambers (Dordrecht: Kluwer), 40
Hartquist, T. W., & Dyson, J. E. 1997, A&A, 319, 589
Healy, A. P., & Huggins, P. J. 1990, AJ, 100, 511
Henney, W. J. 2001, Rev. Mex. AA Ser. Conf., 10, 57
Henney, W. J., Arthur, S. J., & García-Díaz, M. T. 2005a, ApJ, in press
Henney, W. J., Arthur, S. J., Williams, R. J. R., & Ferland, G. J. 2005b, ApJ, 621, 328
Henry, R. B. C., Kwitter, K. B., & Dufour, R. J. 1999, ApJ, 517, 782
Holtzman, J. A., Burrows, C. J., Castertano, S., Hester, J. J., Trauger, J. T., Watson, A. M., & Worthey, G. 1995, PASP, 107, 1065
Huggins, P. J., Bachiller, R., Cox, P., & Forveille, T. 1992, ApJ, 401, L43
Huggins, P. J., Forveille, T., Bachiller, R., Cox, P., Ageorges, N., & Walsh, J. R. 2002, ApJ, 573, L55 (H02)
Huggins, P. J., & Healy, A. P. 1986, ApJ, 305, L29
Johnstone, D., Hollenbach, D., & Bally, J. 1998, ApJ, 499, 758
Leahy, D. A., Zhang, C. Y., & Kwok, S. 1994, ApJ, 422, 205
Lim, A. J., & Mellema, G. 2003, A&A, 405, 189
López-Martín, L., Raga, A. C., Mellema, G., Henney, W. J., & Cantó, J. 2001, ApJ, 548, 288
McCaughrean, M. J., & O'Dell, C. R. 1996, AJ, 111, 1977
Meaburn, J., Clayton, C. A., Bryce, M., Walsh, J., Holloway, A. J., & Steffen, W. 1998, MNRAS, 294, 201 (M98)
Meaburn, J., Walsh, J. R., Clegg, R. E. S., Walton, N. A., & Taylor, D. 1992, MNRAS, 255, 177 (M92)
Mellema, G., Raga, A. C., Cantó, J., Lundqvist, P., Balick, B., Steffen, W., & Noriega-Crespo, A. 1998, A&A, 331, 335
Natta, A., & Hollenbach, D. 1998, A&A, 337, 517 (NH98)
O'Dell, C. R. 1998, AJ, 116, 1346 (O98)
———. 2000, AJ, 119, 2311
O'Dell, C. R., Balick, B., Hajian, A. R., Henney, W. J., & Henney, W. J. 2002, AJ, 123, 3329 (O02)
O'Dell, C. R., & Burkert, A. 1997, in IAU Symp. 180, Planetary Nebulae, ed. H. J. Habing & H. J. G. L. M. Lamers (Dordrecht: Kluwer), 332 (OB97)
O'Dell, C. R., & Doi, T. 1999, PASP, 111, 1316
O'Dell, C. R., & Handron, K. D. 1996, AJ, 111, 1630 (OH96)
O'Dell, C. R., Henney, W. J., & Burkert, A. 2000, AJ, 119, 2910 (OHB00)
O'Dell, C. R., McCullough, P. R., & Meixner, M. 2004, AJ, 128, 2339 (OMM04)
Osterbrock, D. E. 1989, Astrophysics of Gaseous Nebulae and Active Galactic Nuclei (Mill Valley: University Science Books)
Rodríguez, L. F., Goss, W. M., & Williams, R. 2002, ApJ, 574, 179
Sodroski, T. J., et al. 1994, ApJ, 428, 638
Speck, A. K., Meixner, M., Fong, D., McCullough, P. R., Moser, D. E., & Ueta, T. 2002, AJ, 123, 346 (S02)
Speck, A. K., Meixner, M., Jacoby, G. H., & Knezek, P. M. 2003, PASP, 115, 170 (S03)
Thompson, R. I., Rieke, M., Schneider, G., Hines, D. C., & Corbin, M. R. 1998, ApJ, 492, L95
Tielens, A. G. G. M., Meixner, M. M., van der Werf, P. P., Bregman, J., Tauber, J. A., Stutzki, J., & Rank, D. 1993, Science, 262, 86
Vicini, B., Natta, A., Marconi, A., Testi, L., Hollenbach, D., & Draine, B. T. 1999, A&A, 342, 823
Vorontzov-Velyaminov, B. A. 1968, in IAU Symp. 34, Planetary Nebulae, ed. D. E. Osterbrock & C. R. O'Dell (Dordrecht: Reidel), 256
Wood, K., Mathis, J. S., & Ercolano, B. 2004, MNRAS, 348, 1337
Woodgate, B. E., et al. 1998, PASP, 110, 1183
Young, K., Cox, P., Huggins, P. J., Forveille, T., & Bachiller, R. 1999, ApJ, 522, 387 (Y99)
Zanstra, H. 1955, Vistas Astron., 1, 256
Zhang, C. Y., Leahy, D. A., & Kwok, S. 1993, Rev. Mex. AA, 27, 219